Sequence Domain SISO Equivalent Models of a Grid-Tied Voltage Source Converter System for Small-Signal Stability Analysis

Chen Zhang, Xu Cai, Atle Rygg, and Marta Molinas, *Member, IEEE*

***Abstract*—This paper presents a generalized method for converting multi-input and multi-output (MIMO) *dq* impedance model of a grid-tied voltage source converter system into its sequence domain single-input and single-output (SISO) equivalents. As a result, two types of SISO impedance models were derived, one of which was derived from relatively strong and *dq* symmetric grid assumption (reduced SISO model) and the other was based on closed-loop equivalent (accurate SISO model). It was proven that the accurate SISO model has the same marginal stability condition as the MIMO model. Accuracy of these models is assessed with respect to the measured impedances in PSCAD/EMTDC simulations, their effects on stability are analyzed as well. Findings show that the accurate SISO model presents identical stability conclusions as the MIMO model. However, the reduced SISO model may lead to inaccurate results if the system is highly dq asymmetric, e.g., VSC with fast phase-locked loop or an actively controlled grid.**

***Index Terms*—Couplings, PLL, sequence impedance, stability analysis, voltage source converter.**

I. Introduction

NOWADAYS, voltage source converters (VSC) have become widely used in grid-integrated renewable energies [1] and flexible power transmission systems [2]. Oscillations at both low [3] and high frequencies [4] were observed in VSC-based systems, particularly in weak grid conditions [5]. Such types of small-signal stability issues can be effectively assessed by impedance-based analysis. Impedance models of three-phase VSCs [6]–[9], single-phase VSCs [10], and modular multi-level converters [11], among others, have been developed rigorously in recent literature.

For typical two-level and three-phase grid-tied VSCs, the impedance can be extracted either in dq synchronously rotating frame [7] or in three-phase stationary frame [8]. In dq frame, the grid-tied VSC system is time invariant if grid is three-phase balanced. This setup allows for direct linearization; thus, performing Laplace transformation on the resultant linear time invariant (LTI) model yields dq impedances [9]. However, if applied to three-phase stationary frame, the grid-tied VSC inherently varies by time. Therefore, the harmonic linearization method from a previous study [12] is applied to obtain sequence impedances [8]. Generally, linearizing the time-varying system along a steady periodic trajectory yields a linear time periodic (LTP) system. To transform LTP systems into frequency domain, the harmonic balance approach [13] can be adopted.

Despite the different models in dq and sequence domains, both are coupled because of the off-diagonal terms in impedance matrices are nonzero. Recent research has presented interest in the interpretation of these couplings and their consequences during stability assessment. Previous works [14], [15] established that frequency couplings can be identified in their sequence domain (i.e., positive and negative sequences are coupled and separated by twice fundamental frequency); and their impacts on low-frequency stability were also emphasized. This interesting property of VSC was also identified from dq impedance and introduced as dq asymmetry in [16]. Moreover, the relationship between dq and sequence impedances were thoroughly investigated in [17], and findings showed that dq impedances can be transformed into its modified sequence domain equivalents by means of symmetrical decomposition [18]. On the other hand, a complex space vector method [16] is used to directly derive VSC impedance in stationary frame [19].

However, frequency couplings in the foregoing reviews (e.g., [14]–[17]) were in single-frequency coupling form (i.e., a single-frequency perturbation induces a single-frequency coupling that separated by twice the fundamental frequency). This condition is true if either the converter or the grid impedance is dq asymmetric [16] or equivalently contains the mirror frequency coupling effect [17]. If the system is three-phase unbalanced, there will be multiple frequency couplings. To include these couplings with full accuracy, the harmonic-state space [20] as well as the harmonic transfer function method [13] should be adopted.

Currently, both cases on single- and multiple-frequency couplings can only be captured by matrix-based impedances, which are multi-input and multi-output (MIMO) systems by nature; therefore, the generalized Nyquist criterion (GNC) [21] should be adopted for stability analysis. Furthermore, finding the

Manuscript received April 24, 2017; revised July 9, 2017 and September 5, 2017; accepted October 18, 2017. Date of publication November 1, 2017; date of current version May 17, 2018. This work was supported by grants from the Power Electronics Science and Education Development Program of the Delta Environmental and Educational Foundation (DREM2016005). Paper no. TEC-00310-2017. *(Corresponding author: Chen Zhang.)*

C. Zhang and X. Cai are with the Department of Electrical Engineering, Shanghai Jiao Tong University, Shanghai 200240, China (e-mail: nealbc@sjtu.edu.cn; xucai@sjtu.edu.cn).

A. Rygg and M. Molinas are with the Department of Engineering Cybernetics, Norwegian University of Science and Technology, Trondheim 7491, Norway (e-mail: atle.rygg@ntnu.no; marta.molinas@ntnu.no).

Color versions of one or more of the figures in this paper are available online at http://ieeexplore.ieee.org.

Digital Object Identifier 10.1109/TEC.2017.2766217

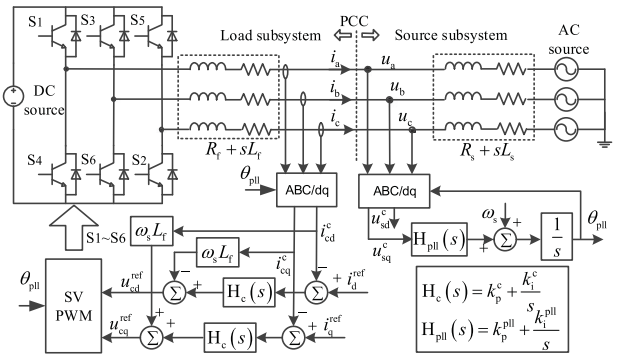

Fig. 1. Schematic of the grid-tied VSC system.

single-input and single-output (SISO) equivalents of grid-tied VSC system is appealing due to their simplicity and convenience for physical interpretation.

This paper aims to develop a generalized method for converting MIMO dq impedance into its sequence domain SISO equivalents by exploring the properties of single-frequency coupling system. The rest of the paper is organized as follows: In Section II, the method for converting the dq impedance into its MIMO sequence domain equivalents is introduced. System blocks of a grid-tied VSC system are modeled based on this method. In Section III, sequence domain MIMO model of grid-tied VSC system is established by assembling the blocks in Section II. And its SISO equivalents are found by performing closed-loop analysis of the entire system, instead of viewing them as subsystems. A detailed comparison of SISO models with measured impedances in PSCAD/EMTDC is presented. Section IV discussed the performance of proposed SISO models in predicting small signal stability. Finally, Section V draws the conclusions.

II. Modeling of Grid-Tied VSC in Modified Sequence Domain

A. Topology and Control Scheme of the Grid-Tied VSC

Fig. 1 presents the system analyzed in this paper. It constitutes a typical two-level VSC, an L-type filter, and a Thevenin-equivalent grid.

Only current controller and phase-locked loop (PLL) are considered, mainly to achieve simplicity of subsequent property analysis. It will not affect the generality of proposed method as will be presented later. Grid voltage feedforwards can have a great impacts on both transient [6] and small-signal response [5] of VSC, if the bandwidths of these feedforwards are not carefully chosen. In this regard, feedforwards are viewed as impedance-shaping method, and will not be discussed in this paper because the focus is on modeling.

B. Symmetrical Decomposition of a dq Impedance

Taking a dq impedance model in [9] as an example,

$$\begin{bmatrix} U_{\rm d}(s) \\ U_{\rm q}(s) \end{bmatrix} = \begin{bmatrix} {\rm Z}^{\rm dd}(s) & {\rm Z}^{\rm dq}(s) \\ {\rm Z}^{\rm qd}(s) & {\rm Z}^{\rm qq}(s) \end{bmatrix} \begin{bmatrix} I_{\rm d}(s) \\ I_{\rm q}(s) \end{bmatrix} \quad (1)$$

Expression (1) is a LTI system and a complex exponential input (e.g.,e^{st}) leads to an output with the same formation [13]. Thus, the variables for dq currents and voltages in (1) can be written explicitly with variable s, as shown below.

$$\begin{bmatrix} \mathbf{U}_{\rm d} \\ \mathbf{U}_{\rm q} \end{bmatrix} e^{st} = \begin{bmatrix} {\rm Z}^{\rm dd}(s) & {\rm Z}^{\rm dq}(s) \\ {\rm Z}^{\rm qd}(s) & {\rm Z}^{\rm qq}(s) \end{bmatrix} \begin{bmatrix} \mathbf{I}_{\rm d} \\ \mathbf{I}_{\rm q} \end{bmatrix} e^{st}, \forall s \to {\rm j}\omega \quad (2)$$

where $s \to {\rm j}\omega$ is translated from s-domain to frequency-domain. $\mathbf{I}_{\rm d}, \mathbf{I}_{\rm q}$ and $\mathbf{U}_{\rm d}, \mathbf{U}_{\rm q}$ are the current and voltage phasors at frequency ω respectively, and they can be decomposed as:

$$\begin{bmatrix} \mathbf{U}_{\rm p} \\ \mathbf{U}_{\rm n} \end{bmatrix} = \frac{1}{2} \begin{bmatrix} 1 & {\rm j} \\ 1 & -{\rm j} \end{bmatrix} \begin{bmatrix} \mathbf{U}_{\rm d} \\ \mathbf{U}_{\rm q} \end{bmatrix} = \mathbf{A} \begin{bmatrix} \mathbf{U}_{\rm d} \\ \mathbf{U}_{\rm q} \end{bmatrix} \quad (3)$$

Applying matrix $\mathbf{A}$ and its inverse $\mathbf{A}^{-1}$ to (2) yields:

$$\begin{aligned} \begin{bmatrix} \mathbf{U}_{\rm p} \\ \mathbf{U}_{\rm n} \end{bmatrix} &= \mathbf{A} \begin{bmatrix} {\rm Z}^{\rm dd}(s) & {\rm Z}^{\rm dq}(s) \\ {\rm Z}^{\rm qd}(s) & {\rm Z}^{\rm qq}(s) \end{bmatrix} \mathbf{A}^{-1} \begin{bmatrix} \mathbf{I}_{\rm p} \\ \mathbf{I}_{\rm n} \end{bmatrix} \\ &= \mathbf{Z}^{\rm PN}(s) \begin{bmatrix} \mathbf{I}_{\rm p} \\ \mathbf{I}_{\rm n} \end{bmatrix}, \forall s \to {\rm j}\omega \end{aligned} \quad (4)$$

where elements in $\mathbf{Z}^{\rm PN}(s) = \left[\begin{smallmatrix} {\rm Z}^{\rm dd}(s) & {\rm Z}^{\rm dq}(s) \\ {\rm Z}^{\rm qd}(s) & {\rm Z}^{\rm qq}(s) \end{smallmatrix}\right]$ are generally complex transfer functions. This method makes it possible to obtain the *modified* sequence impedance directly from well-developed dq impedance as discussed in [17] (i.e., the same authors of this paper). The term "modified" denotes the specific frequency notation used in [17], where the frequency of sequence impedances is referred to dq frame. This notation is adopted in the present paper as well, and the term "modified" will be omitted for brevity in subsequent analysis. However, other recent works e.g., [14] and [19] use a different frequency notation, which are referred to phase domain.

C. Sequence Domain System Blocks of Grid-Tied VSC

Adopting the decomposition method in Section II-B, system blocks of a grid-tied VSC system in dq format (e.g., [9]) can be transformed into their sequence domain equivalents.

For passive circuit elements, e.g., filter:

$$\begin{bmatrix} R_{\rm f} + sL_{\rm f} & -\omega_{\rm s}L_{\rm f} \\ \omega_{\rm s}L_{\rm f} & R_{\rm f} + sL_{\rm f} \end{bmatrix} \overset{\rm dq-pn}{\to} \begin{bmatrix} {\rm Z}_{\rm f}^{\rm pp}(s) & 0 \\ 0 & {\rm Z}_{\rm f}^{\rm nn}(s) \end{bmatrix} \quad (5)$$

where ${\rm Z}_{\rm f}^{\rm pp}(s) = R_{\rm f} + sL_{\rm f} + {\rm j}\omega_{\rm s}L_{\rm f}$, ${\rm Z}_{\rm f}^{\rm nn}(s) = \bar{\rm Z}_{\rm f}^{\rm pp}(s)$. The upper line on the latter denotes complex-conjugate operator on the function (i.e., the coefficients not the Laplace variable "s"). For a typical Thevenin grid, its sequence impedances are similarly as the filter, which are ${\rm Z}_{\rm s}^{\rm pp}(s) = R_{\rm s} + sL_{\rm s} + {\rm j}\omega_{\rm s}L_{\rm s}$ and ${\rm Z}_{\rm s}^{\rm nn}(s) = \bar{\rm Z}_{\rm s}^{\rm pp}(s)$ respectively.

For variables perturbed by abc to dq transformation e.g., converter output currents:

$$\begin{bmatrix} 0 & \frac{I_{\rm cq0}{\rm T}_{\rm pll}(s)}{U_0} \\ 0 & -\frac{I_{\rm cd0}{\rm T}_{\rm pll}(s)}{U_0} \end{bmatrix} \overset{\rm dq-pn}{\to} \frac{{\rm T}_{\rm pll}(s)}{2U_0} \begin{bmatrix} -\underline{I}_{\rm c0} & \underline{I}_{\rm c0} \\ \underline{I}_{\rm c0}^* & -\underline{I}_{\rm c0}^* \end{bmatrix} \quad (6)$$

where ${\rm T}_{\rm pll}(s) = \frac{U_0{\rm H}_{\rm pll}(s)}{s + U_0{\rm H}_{\rm pll}(s)}$ is the closed-loop system of a typical PLL as in Fig. 1. U_0 is the voltage at PLL sampling point.

$\underline{I}_{c0} = I_{cd0} + jI_{cq0}$ is the complex-valued current in steady. The converter output voltage can be obtained similarly as: $\frac{T_{pll}(s)}{2U_0}\begin{bmatrix} -\underline{U}_{c0} & \underline{U}_{c0} \\ \underline{U}^*_{c0} & -\underline{U}^*_{c0} \end{bmatrix}$. $\underline{U}_{c0} = U_{cd0} + jU_{cq0}$ is the complex-valued converter terminal voltage.

For current controller it has:

$$\begin{bmatrix} H_c(s) & 0 \\ 0 & H_c(s) \end{bmatrix} \overset{dq-pn}{\rightarrow} \begin{bmatrix} H_c^{pp}(s) & 0 \\ 0 & H_c^{nn}(s) \end{bmatrix} \tag{7}$$

Generally, all the system blocks in dq domain can be transformed into their sequence domain equivalents, e.g., VSC with PQ controller, DC voltage controller etc.

D. Sequence Impedance Model of the Grid-Tied VSC System

The sequence domain MIMO model of a grid-tied VSC system can be established by assembling system blocks derived in Section II-C.

For a load (VSC) subsystem, its admittance is:

$$-\begin{bmatrix} \mathbf{i}_L^p \\ \mathbf{i}_L^n \end{bmatrix} = \begin{bmatrix} Y_L^{pp}(s) & Y_L^{pn}(s) \\ Y_L^{np}(s) & Y_L^{nn}(s) \end{bmatrix}\begin{bmatrix} \mathbf{u}_L^p \\ \mathbf{u}_L^n \end{bmatrix} = \mathbf{Y}_L^{PN}(s)\begin{bmatrix} \mathbf{u}_L^p \\ \mathbf{u}_L^n \end{bmatrix} \tag{8}$$

For a generalized source (grid) subsystem, its impedance is:

$$\begin{bmatrix} \mathbf{u}_S^p \\ \mathbf{u}_S^n \end{bmatrix} = \begin{bmatrix} Z_S^{pp}(s) & Z_S^{pn}(s) \\ Z_S^{np}(s) & Z_S^{nn}(s) \end{bmatrix}\begin{bmatrix} \mathbf{i}_S^p \\ \mathbf{i}_S^n \end{bmatrix} = \mathbf{Z}_S^{PN}(s)\begin{bmatrix} \mathbf{i}_S^p \\ \mathbf{i}_S^n \end{bmatrix} \tag{9}$$

$$\mathbf{i}_S^p = \mathbf{i}_L^p, \mathbf{i}_S^n = \mathbf{i}_L^n \tag{10}$$

$$\mathbf{u}_S^p + \mathbf{u}_{ptb}^p = \mathbf{u}_L^p, \mathbf{u}_L^n = \mathbf{u}_S^n \tag{11}$$

where $Y_L^{pp} = \frac{1-G_{pll}}{H_c^{pp}+Z_f^{pp}}$, $Y_L^{nn} = \bar{Y}_L^{pp}$, $Y_L^{pn} = \frac{G_{pll}}{H_c^{pp}+Z_f^{pp}}$, $Y_L^{np} = \bar{Y}_L^{pn}$ and $G_{pll} = \frac{T_{pll}}{2U_0}(H_c\underline{I}_{c0} + \underline{U}_{c0})$. Laplace variable s is omitted for brevity.

$\mathbf{u}_{ptb}^p$ is a positive sequence perturbation voltage. Functions in bold format e.g., $\mathbf{Z}_S^{PN}$ denotes a matrix, in the case of Fig. 1, it has $Z_S^{pn}(s) = Z_S^{np}(s) = 0$, as the grid is passive and dq symmetric. The subscript 'S' in capital format denotes source (e.g., grid) subsystem, and 'L' denotes load (e.g., VSC) subsystem. Note that the line on the letter e.g., $\bar{Y}_L^{pp}$ is conjugate operator on the function, if the full complex conjugate operator "$*$" is used, it has $(Y_L^{pp})^* = \bar{Y}_L^{pp}(\bar{s})$. The derived MIMO model as (8) and (9) can be used directly to assess small-signal stability with the help of GNC [14]. A previous study [17] proved that the GNC based on this model leads to identical results, as the GNC based on dq impedance.

The sequence equivalent circuits can be plotted as Fig. 2 on the basis of (8)–(11). In Fig. 2, positive and negative sequence circuits are coupled via two dependent current sources, which are voltage controlled. This intrinsic binding between positive and negative sequence circuits will be explored further in next section for finding their SISO equivalents.

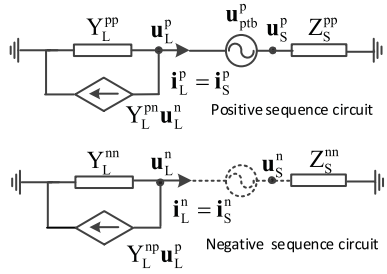

Fig. 2. Sequence domain equivalent circuits of the grid-tied VSC system.

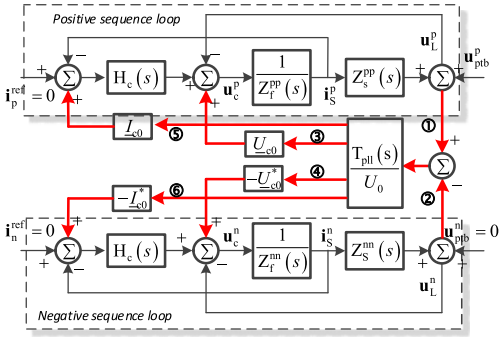

Fig. 3. Sequence domain control blocks diagram of a grid-tied VSC system.

III. SISO Equivalent Models of a Grid-Tied VSC System

A. Analysis of Coupled Sequence Loops

In order to reveal the sequence coupling in a more intuitive way, manipulating the system blocks (5)–(7) with electrical system configuration in Fig. 1 yields Fig. 3.

Fig. 3 clearly identifies the positive and negative sequence loops coupled via six paths, which are all caused by the PLL (i.e., $T_{pll}(s)$). Different paths will result in models with different accuracies, as in the following cases:

Case 1: By neglecting all paths, the simplest model with decoupled positive and negative sequences is obtained. Although this case may not be effective for stability analysis, it is useful for identifying the intrinsic properties of the grid-VSC system (e.g., resonant point), and the coupling effects of PLL can be introduced as additional damping sources to the intrinsic resonant point [22].

Case 2: By isolating the paths of ①③⑤ and ②④⑥, another popular decoupled sequence model as in [8] is obtained. The positive and negative loop impedance from perturbation voltage to the current response can be calculated directly from Fig. 3; i.e., $1/Y_L^{pp} + Z_S^{pp}$ and $1/Y_L^{nn} + Z_S^{nn}$. Note that the obtained loop impedance is equivalent to neglect the off-diagonal terms in the converter admittance. This condition is satisfied if the grid is relatively strong and dq symmetric. See the proof in the subsequent analysis as in (18), (19).

The foregoing analysis presents two decoupled models for the grid-tied VSC, which are SISO systems. However, both models neglect sequence coupling to some extent. In the following section, we will develop a method for deriving an accurate SISO model with no assumptions and reductions.

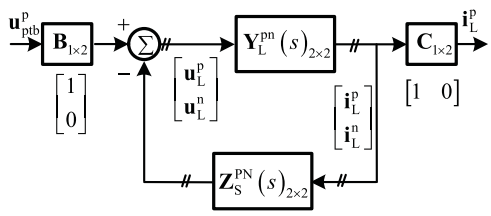

Fig. 4. Closed-loop representation of a grid-tied VSC system.

B. Accurate and Reduced SISO Models of the Grid-Tied VSC

In this subsection, we regard VSC and grid as a closed-loop system, not as subsystems, perturbed by independent sources. Due to linearity, closed-loop analysis under positive and negative independent perturbations can be analyzed separately.

Taking the positive sequence as an example, the positive sequence loop impedance can be obtained by solving the linear system in Fig. 4:

$$\mathrm{Z}^{\mathrm{P}}_{\mathrm{Loop}}\left(\mathrm{s}\right)=-\frac{\mathbf{u}^{\mathrm{p}}_{\mathrm{ptb}}}{\mathbf{i}^{\mathrm{p}}_{\mathrm{L}}}=\frac{1}{\mathbf{C}\left(\mathbf{Z}^{\mathrm{PN}}_{\mathrm{L}}\left(s\right)+\mathbf{Z}^{\mathrm{PN}}_{\mathrm{S}}\left(s\right)\right)^{-1}\mathbf{B}} \tag{12}$$

where $\mathbf{Z}^{\mathrm{PN}}_{\mathrm{L}}(s)=(\mathbf{Y}^{\mathrm{PN}}_{\mathrm{L}}(s))^{-1}$. It should be noted that the derived loop impedance is one dimension, i.e., a SISO system.

Substituting elements as in (8) and (9) into (12) yields:

$$\mathrm{Z}^{\mathrm{P}}_{\mathrm{Loop}}\left(s\right)=\mathrm{Z}^{\mathrm{pp}}_{\mathrm{S}}+\mathrm{Z}^{\mathrm{pp}}_{\mathrm{L}}-\frac{\left(\mathrm{Z}^{\mathrm{np}}_{\mathrm{L}}+\mathrm{Z}^{\mathrm{np}}_{\mathrm{S}}\right)\left(\mathrm{Z}^{\mathrm{pn}}_{\mathrm{L}}+\mathrm{Z}^{\mathrm{pn}}_{\mathrm{S}}\right)}{\mathrm{Z}^{\mathrm{nn}}_{\mathrm{S}}+\mathrm{Z}^{\mathrm{nn}}_{\mathrm{L}}} \tag{13}$$

This method is applied to find the negative sequence loop impedance. Replacing the matrix $\mathbf{B}=[0\ 1]^{T}$,$\mathbf{C}=[0\ 1]$ and $\mathbf{u}^{\mathrm{p}}_{\mathrm{ptb}}\rightarrow\mathbf{u}^{\mathrm{n}}_{\mathrm{ptb}}$ yields:

$$\mathrm{Z}^{\mathrm{N}}_{\mathrm{Loop}}\left(s\right)=\mathrm{Z}^{\mathrm{nn}}_{\mathrm{S}}+\mathrm{Z}^{\mathrm{nn}}_{\mathrm{L}}-\frac{\left(\mathrm{Z}^{\mathrm{pn}}_{\mathrm{L}}+\mathrm{Z}^{\mathrm{pn}}_{\mathrm{S}}\right)\left(\mathrm{Z}^{\mathrm{np}}_{\mathrm{L}}+\mathrm{Z}^{\mathrm{np}}_{\mathrm{S}}\right)}{\mathrm{Z}^{\mathrm{pp}}_{\mathrm{S}}+\mathrm{Z}^{\mathrm{pp}}_{\mathrm{L}}} \tag{14}$$

Expressions (13) and (14) is defined as the *accurate SISO model*, and $\mathrm{Z}^{\mathrm{P}}_{\mathrm{Loop}}(s)=\bar{\mathrm{Z}}^{\mathrm{N}}_{\mathrm{Loop}}(s)$ still holds, i.e., if we have the analytical model of the positive sequence, the negative sequence model is determined accordingly. In addition, during the derivation, no assumption for dq symmetry was made, therefore this method is general for any LTI systems.

The physical interpretation of this method is: the negative sequence circuit in Fig. 2 is augmented into the positive sequence network (and vice versa) via the voltage-controlled dependent current source. Consequently, the effects of sequence coupling are included in this model intrinsically.

In order to proof the validity of the method, a previous work in [17], where the sequence impedance is derived for source and load subsystem is compared. Taking the positive sequence model for example, in [17] it has:

$$\mathrm{Z}^{\mathrm{p}}_{\mathrm{L}}=-\frac{\mathbf{u}^{\mathrm{p}}_{\mathrm{L}}}{\mathbf{i}^{\mathrm{p}}_{\mathrm{L}}}=\mathrm{Z}^{\mathrm{pp}}_{\mathrm{L}}-\frac{\mathrm{Z}^{\mathrm{pn}}_{\mathrm{L}}\left(\mathrm{Z}^{\mathrm{np}}_{\mathrm{L}}+\mathrm{Z}^{\mathrm{np}}_{\mathrm{S}}\right)}{\mathrm{Z}^{\mathrm{nn}}_{\mathrm{S}}+\mathrm{Z}^{\mathrm{nn}}_{\mathrm{L}}} \tag{15}$$

$$\mathrm{Z}^{\mathrm{p}}_{\mathrm{S}}=\frac{\mathbf{u}^{\mathrm{p}}_{\mathrm{S}}}{\mathbf{i}^{\mathrm{p}}_{\mathrm{S}}}=\mathrm{Z}^{\mathrm{pp}}_{\mathrm{S}}-\frac{\mathrm{Z}^{\mathrm{pn}}_{\mathrm{S}}\left(\mathrm{Z}^{\mathrm{np}}_{\mathrm{L}}+\mathrm{Z}^{\mathrm{np}}_{\mathrm{S}}\right)}{\mathrm{Z}^{\mathrm{nn}}_{\mathrm{S}}+\mathrm{Z}^{\mathrm{nn}}_{\mathrm{L}}} \tag{16}$$

$$\begin{aligned}\mathrm{Z}^{\mathrm{n}}_{\mathrm{L}}\left(s\right)&=\bar{\mathrm{Z}}^{\mathrm{p}}_{\mathrm{L}}\left(s\right)\\ \mathrm{Z}^{\mathrm{n}}_{\mathrm{S}}\left(s\right)&=\bar{\mathrm{Z}}^{\mathrm{p}}_{\mathrm{S}}\left(s\right)\end{aligned} \tag{17}$$

We can clearly observe that $\mathrm{Z}^{\mathrm{p}}_{\mathrm{L}}+\mathrm{Z}^{\mathrm{p}}_{\mathrm{S}}=\mathrm{Z}^{\mathrm{P}}_{\mathrm{Loop}}$ and $\mathrm{Z}^{\mathrm{n}}_{\mathrm{L}}+\mathrm{Z}^{\mathrm{n}}_{\mathrm{S}}=\mathrm{Z}^{\mathrm{N}}_{\mathrm{Loop}}$. ((15) and (16) are equivalent to (33) in [17], but are written in a more compact form with slightly different notation.)

Furthermore, if considering a dq symmetric and relatively strong grid, it has conditions as: $\mathrm{Z}^{\mathrm{pp}}_{\mathrm{S}}=\mathrm{Z}^{\mathrm{np}}_{\mathrm{S}}=0$,$|\mathrm{Z}^{\mathrm{pp}}_{\mathrm{S}}|\ll|\mathrm{Z}^{\mathrm{pp}}_{\mathrm{L}}|,\forall\omega$ and $|\mathrm{Z}^{\mathrm{nn}}_{\mathrm{S}}|\ll|\mathrm{Z}^{\mathrm{nn}}_{\mathrm{L}}|,\forall\omega$. Hence, (13) and (14) can be reduced to:

$$\mathrm{Z}^{\mathrm{P\_rdu}}_{\mathrm{Loop}}\left(s\right)=\mathrm{Z}^{\mathrm{pp}}_{\mathrm{S}}+\frac{\det\left|\mathbf{Z}^{\mathrm{PN}}_{\mathrm{L}}\right|}{\mathrm{Z}^{\mathrm{nn}}_{\mathrm{L}}}=\mathrm{Z}^{\mathrm{pp}}_{\mathrm{S}}+\frac{1}{\mathrm{Y}^{\mathrm{pp}}_{\mathrm{L}}} \tag{18}$$

$$\mathrm{Z}^{\mathrm{N\_rdu}}_{\mathrm{Loop}}\left(\mathrm{s}\right)=\mathrm{Z}^{\mathrm{nn}}_{\mathrm{S}}+\frac{\det\left|\mathbf{Z}^{\mathrm{PN}}_{\mathrm{L}}\right|}{\mathrm{Z}^{\mathrm{pp}}_{\mathrm{L}}}=\mathrm{Z}^{\mathrm{nn}}_{\mathrm{S}}+\frac{1}{\mathrm{Y}^{\mathrm{nn}}_{\mathrm{L}}} \tag{19}$$

Expressions (18) and (19) is defined as the *reduced SISO model*, which is widely applied in previous research [8]. However, a frequency translation to phase domain is needed since this paper uses a dq frequency notation.

C. Proof of Identical Marginal Stability Condition

This subsection will prove that the accurate SISO model is consistent with the MIMO model in terms of marginal stability condition. The marginal stability condition is defined as the case when the eigenvalue loci of a MIMO or SISO system cross the $(-1,0)$ point on the basis of GNC or NC.

For MIMO-based model, the marginal stability condition is:

$$\text{There is } s \text{ that eig}\left(\mathbf{Z}^{\mathrm{PN}}_{\mathrm{S}}\cdot\mathbf{Y}^{\mathrm{PN}}_{\mathrm{L}}\right)\quad\text{equals}\quad-1+0\cdot\mathrm{j} \tag{20}$$

where $\mathbf{Z}^{\mathrm{PN}}_{\mathrm{S}}$, $\mathbf{Y}^{\mathrm{PN}}_{\mathrm{L}}$ are given in (8) and (9). After some calculations, we have the equality as:

$$\begin{aligned}&\det\mathbf{Z}^{\mathrm{PN}}_{\mathrm{S}}+\det\mathbf{Z}^{\mathrm{PN}}_{\mathrm{L}}+\mathrm{Z}^{\mathrm{pp}}_{\mathrm{S}}\mathrm{Z}^{\mathrm{nn}}_{\mathrm{L}}+\mathrm{Z}^{\mathrm{nn}}_{\mathrm{S}}\mathrm{Z}^{\mathrm{pp}}_{\mathrm{L}}-\mathrm{Z}^{\mathrm{np}}_{\mathrm{L}}\mathrm{Z}^{\mathrm{pn}}_{\mathrm{S}}\\ &\quad-\mathrm{Z}^{\mathrm{pn}}_{\mathrm{L}}\mathrm{Z}^{\mathrm{np}}_{\mathrm{S}}=0\end{aligned} \tag{21}$$

For SISO-based model, the marginal stability condition is:

$$\text{There is } s \text{ that eig}\left(\mathrm{Z}^{\mathrm{p}}_{\mathrm{S}}/\mathrm{Z}^{\mathrm{p}}_{\mathrm{L}}\right)\quad\text{equals}\quad-1+0\cdot\mathrm{j} \tag{22}$$

where $\mathrm{Z}^{\mathrm{p}}_{\mathrm{S}},\mathrm{Z}^{\mathrm{p}}_{\mathrm{L}}$ are given in (15) and (16).

(22) is equivalent to $\det|\frac{\mathrm{Z}^{\mathrm{P}}_{\mathrm{Loop}}}{\mathrm{Z}^{\mathrm{p}}_{\mathrm{L}}}|=0\rightarrow\mathrm{Z}^{\mathrm{P}}_{\mathrm{Loop}}=0$, thus the equality given by (13) is:

$$\left(\mathrm{Z}^{\mathrm{nn}}_{\mathrm{S}}+\mathrm{Z}^{\mathrm{nn}}_{\mathrm{L}}\right)\left(\mathrm{Z}^{\mathrm{pp}}_{\mathrm{S}}+\mathrm{Z}^{\mathrm{pp}}_{\mathrm{L}}\right)-\left(\mathrm{Z}^{\mathrm{pn}}_{\mathrm{L}}+\mathrm{Z}^{\mathrm{pn}}_{\mathrm{S}}\right)\left(\mathrm{Z}^{\mathrm{np}}_{\mathrm{L}}+\mathrm{Z}^{\mathrm{np}}_{\mathrm{S}}\right)=0 \tag{23}$$

Expanding (23), then substitute $\det\mathbf{Z}^{\mathrm{PN}}_{\mathrm{S}}=\mathrm{Z}^{\mathrm{pp}}_{\mathrm{S}}\mathrm{Z}^{\mathrm{nn}}_{\mathrm{S}}-\mathrm{Z}^{\mathrm{pn}}_{\mathrm{S}}\mathrm{Z}^{\mathrm{np}}_{\mathrm{S}}$ and $\det\mathbf{Z}^{\mathrm{PN}}_{\mathrm{L}}=\mathrm{Z}^{\mathrm{pp}}_{\mathrm{L}}\mathrm{Z}^{\mathrm{nn}}_{\mathrm{L}}-\mathrm{Z}^{\mathrm{pn}}_{\mathrm{L}}\mathrm{Z}^{\mathrm{np}}_{\mathrm{L}}$ into (23) can prove that (21) equals (23), i.e., the accurate SISO model has the same marginal stability condition as the MIMO model. Therefore it can be used with accuracy in stability analysis. Furthermore, any modifications on SISO model will lead to a marginal stability condition different from (23) e.g., the reduced SISO model. Note that the same proof applies to the negative sequence.

D. Comparison of SISO Models with Measurements

The accurate SISO model as in (13) and (14), and the reduced SISO model as in (18) and (19), will be compared under conditions of a) dq symmetric and b) dq asymmetric grid.

Impedance measurements conducted in PSCAD/EMTDC with the system in Fig. 1 (see Appendix A for detailed

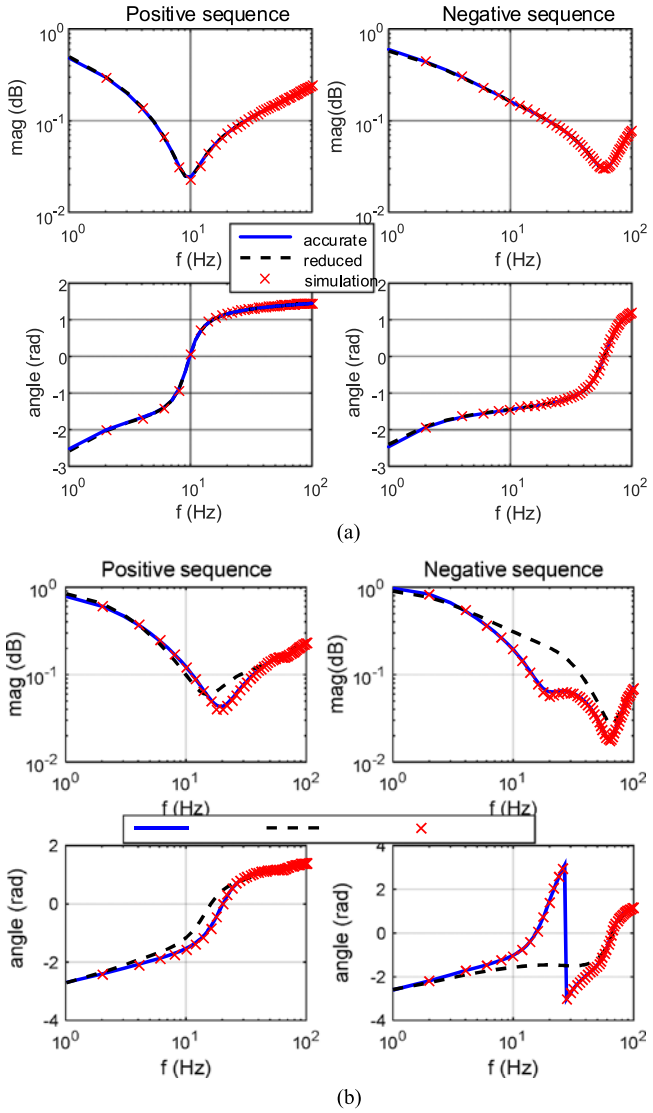

Fig. 5. Loop impedance comparison under dq symmetric grid. (a) SCR = 4, CC = 200 Hz, PLL = 5 Hz, current is 0.5 p.u. (flow out). (b) SCR = 4, CC = 200 Hz, PLL = 200 Hz, current is 0.5 p.u. (flow out).

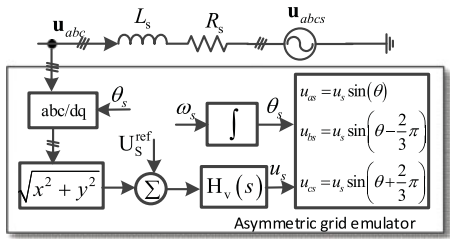

Fig. 6. Control scheme for asymmetric grid emulation.

system parameters). The multi-run module in PSCAD is used. At each run, a single-tone harmonic voltage is injected into the grid. The frequency is varied from 0 Hz to 100 Hz with an increment of 2 Hz. The sampling frequency and sampling window used for Fourier analysis are 1 kHz and 0.5 s respectively. All data and figures are post-processed in MATLAB.

1) dq *Symmetric Grid Cases:* As shown in Fig. 5(a), both accurate and reduced SISO models achieved a good match with

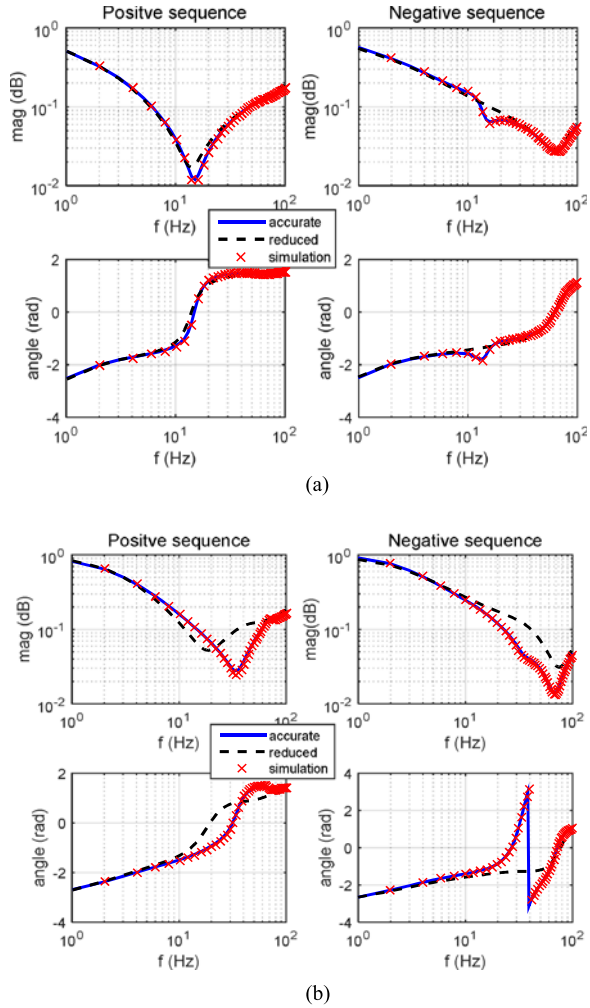

Fig. 7. Loop impedance comparison under dq asymmetric grid. (a) SCR = 4, CC = 200 Hz, PLL = 5 Hz, current is 0.5 p.u. (flow out) (Note that SCR here is only used for calculating grid passive impedance). (b) SCR = 4, CC = 200 Hz, PLL = 300 Hz, current is 0.5 p.u. (flow out) (Note that SCR here is only used for calculating grid impedance).

the measured impedances under a slow PLL configuration. However, if PLL bandwidth is increased to a relatively large value, the shapes of the reduced model would differ from the measurements, particularly for the negative sequence impedances, as shown in Fig. 5(b). By contrast, the accurate SISO model tracks the measured impedances accurately in Fig. 5(b). It proves that the accurate SISO model is superior to the reduced SISO model in capturing the details of impedance characteristics.

2) dq *Asymmetric Grid Cases:* In this paragraph, an actively controlled grid is introduced to emulate the asymmetric behavior in source subsystem.

The control scheme is shown in Fig. 6, where $\omega_s = 2\pi \cdot 50$ is constant, $\mathrm{U_s^{ref}}$ is the voltage amplitude set point of the active grid. $\mathrm{H_v}(s) = k_\mathrm{p}^\mathrm{v} + \frac{k_\mathrm{i}^\mathrm{v}}{s}$ is the voltage regulator. The sequence impedance of the actively controlled grid is asymmetric and can be found in Appendix. B ((A.1) and (A.2)).

Comparing Fig. 7(a) with Fig. 6(a) we can identify that, the good accuracy of reduced SISO model under symmetric grid as well as slow PLL configuration is violated if dq asymmetric

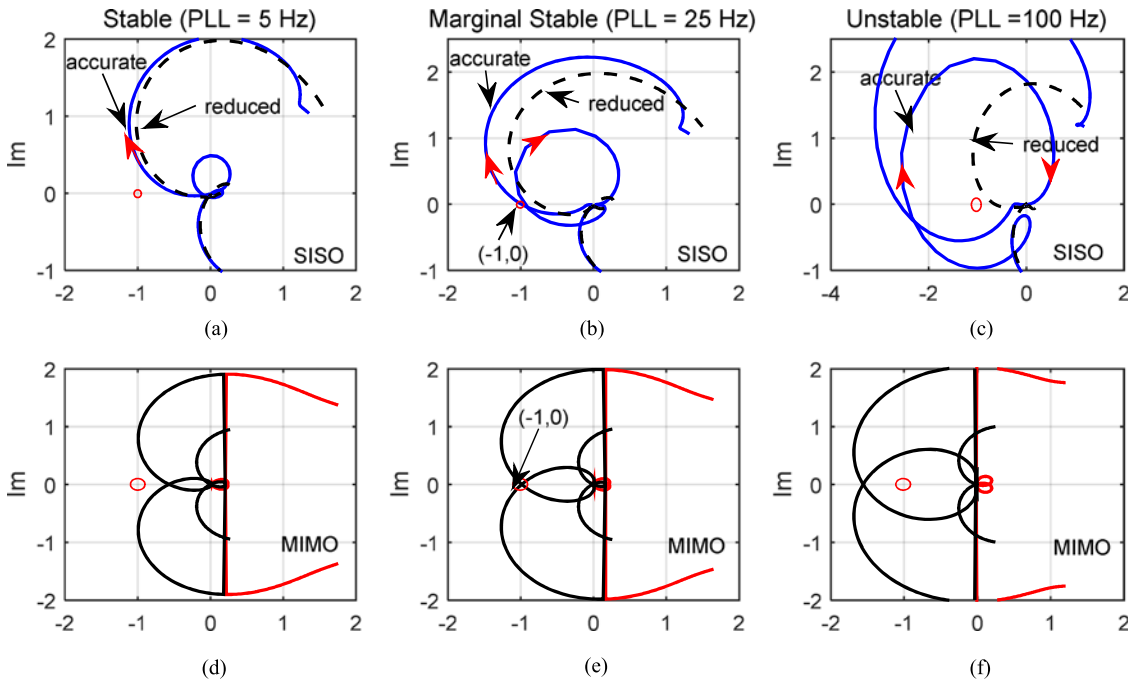

Fig. 8. Numerical stability comparisons with an asymmetric grid (SCR = 4, CC = 200 Hz, current is 0.5 p.u., dash line denotes locus of reduced SISO model, solid blue line denotes locus of accurate SISO model).

grid is presented. The inaccuracy of reduced SISO model can be identified clearly in Fig. 7(b) as well, where a fast PLL is adopted. On the contrary, the accurate SISO model still presents good accuracy in all conditions.

IV. Small-Signal Stability Analysis

This section will further analyze the validity of the proposed SISO models in terms of small-signal stability, particularly for the marginal stability condition in Section III-C. By acquiring the advantages of SISO properties, the proposed model can be used in combination with classic Nyquist criterion (NC) [23].

A. Numerical Stability Analysis

Three model and criterion combinations are considered:

1) Reduced SISO with NC. (For comparison)
2) Accurate SISO with NC. (For comparison)
3) MIMO model with GNC. (For Reference).

In a, the eigenvalue loci is obtained straightforward as $\lambda_{\mathrm{P}}(s) = \mathrm{Z}_{\mathrm{S}}^{\mathrm{pp}} \cdot \mathrm{Y}_{\mathrm{L}}^{\mathrm{pp}}$ and $\lambda_{\mathrm{N}}(s) = \mathrm{Z}_{\mathrm{S}}^{\mathrm{nn}} \cdot \mathrm{Y}_{\mathrm{L}}^{\mathrm{pp}}$ in accordance with (18) and (19).

In b, since the SISO loop impedance in (13) can be decomposed into source and load subsystems as (15) and (16). Therefore, the eigenvalue loci of minor loop gains are $\lambda_{\mathrm{P}}(s) = \mathrm{Z}_{\mathrm{S}}^{\mathrm{p}}/\mathrm{Z}_{\mathrm{L}}^{\mathrm{p}}$ and $\lambda_{\mathrm{N}}(s) = \mathrm{Z}_{\mathrm{S}}^{\mathrm{n}}/\mathrm{Z}_{\mathrm{L}}^{\mathrm{p}}$, where $\mathrm{Z}_{\mathrm{S}}^{\mathrm{p}}, \mathrm{Z}_{\mathrm{L}}^{\mathrm{p}}, \mathrm{Z}_{\mathrm{S}}^{\mathrm{n}}, \mathrm{Z}_{\mathrm{L}}^{\mathrm{n}}$ are given by (15)–(17).

In c, the eigenvalue loci can be calculated from $\det|\lambda \cdot \mathbf{I} - \mathbf{Z}_{\mathrm{S}}^{\mathrm{PN}}\mathbf{Y}_{\mathrm{L}}^{\mathrm{PN}}(\mathrm{s})| = 0$, where $\lambda_1(s), \lambda_2(s)$ are the two solutions. The abovementioned eigenvalue loci are complex transfer functions; thus, the locus for negative frequencies is not the conjugation of the locus of positive frequencies [16]. However, the eigenvalue loci of SISO systems have the property $(\lambda_{\mathrm{N}}(j\omega))^* = \bar{\lambda}_{\mathrm{N}}(-j\omega) = \lambda_{\mathrm{P}}(-j\omega)$. Hence, the negative frequency plots can be obtained by conjugating the negative sequence locus.

Fig. 8 illustrates the stability comparisons of three model and criterion combinations under a dq asymmetric grid condition. By varying PLL bandwidth in three steps from slow to fast, the system is stable, marginal stable and unstable respectively. The accurate SISO model with NC has the same stability conclusion as the MIMO model with GNC. Particularly, the eigenvalue loci of accurate SISO model and MIMO model cross the $(-1, 0\mathrm{j})$ point simultaneously, indicating that the proof of marginal stability condition in Section III-C is correct. On the other hand, the reduced SISO model fails to give the correct marginal stability condition, as well as the stability conclusion, identified in Figs. 8(b) and (c) respectively.

Therefore, it is not safe to use the reduced SISO model if the converter and grid is highly dq asymmetric. On the contrary, the accurate SISO model is effective for stability analysis in this respect.

The marginal stability can also be analyzed physically by finding the damping characteristic at resonances of loop impedance, e.g., by passivity analysis in [24]. The following time domain study will provide more physical insights into the oscillatory behavior lies in the grid-tied VSC system.

B. Simulation Study

The physical interpretation of marginally stable condition is that the loop impedance has approximately zero damping at a resonance frequency. By plotting the real and imaginary parts of loop impedance, the resonances can be found at frequencies

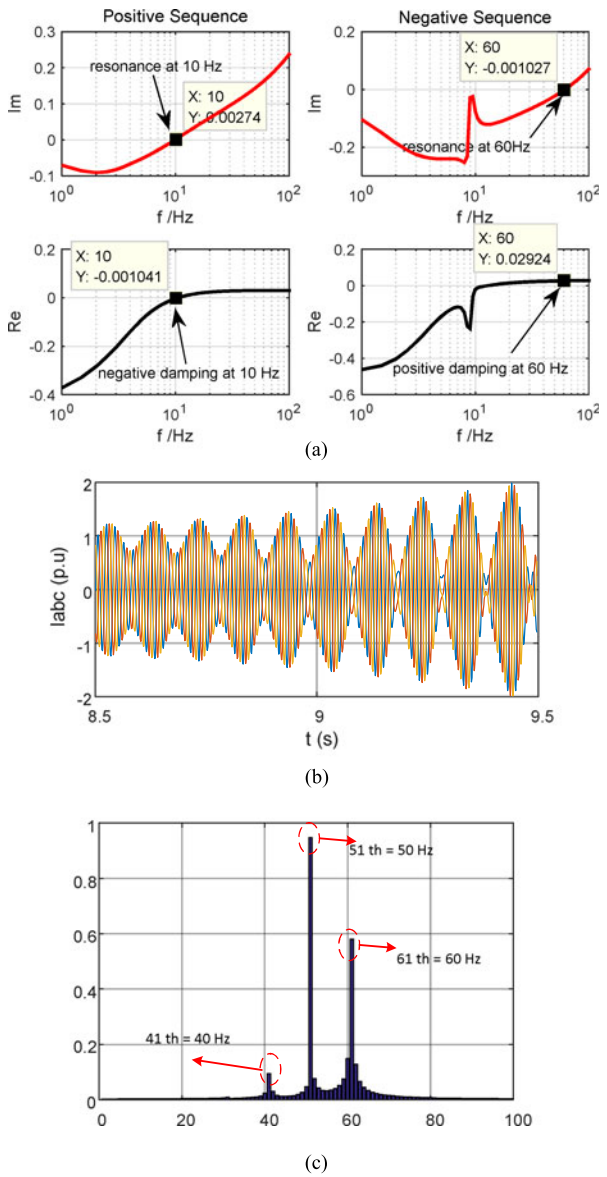

Fig. 9. Marginally stable analysis (CC = 200 Hz SCR = 4, VSC current is 1p.u.). (a) Positive and negative sequence loop impedance plots. (b) Time domain simulation. (Before 2 seconds, the PLL bandwidth is 5 Hz to achieve a stable operational point. Afterwards, the PLL bandwidth is set to 20 Hz. Oscillation is observable after several seconds.). (c) Fourier analysis of phase current. (Sampling rate is 1 kHz. Sampling window is 1 second.)

where the imaginary part cross zero axis, meanwhile damping at these resonances can be determined according to the sign of real parts.

As shown in Fig. 9(a), the positive sequence loop impedance has a resonance at 10 Hz, while the negative sequence loop impedance has a resonance at 60 Hz, this findings is consistent with the analytical calculation of resonant points in [22]. Furthermore, the damping at 10 Hz resonance is negative with small value, indicating a marginally unstable condition, on the contrary a positive damping characteristic is presented at 60 Hz, indicating a stable resonance. It is again emphasized that the resonance frequencies are referred to dq frame in the above analysis.

Time domain simulations in PSCAD/EMTDC also draw similar conclusions in terms of stability. The VSC output currents gradually become unstable during a long simulation time in Fig. 9(b), this is due to the fact that negative damping at 10 Hz is small.

Furthermore, by performing a Fourier analysis on the phase current, we can identify that two additional frequencies except the fundamental at 40 Hz and 60 Hz appears, the *mirror frequency coupling effect* is originated from oscillations in dq frame at 10 Hz, which again proves the correctness of above analysis. Additionally, the oscillatory behavior shown in Fig. 9(b) is also similar to the field measurements of grid-tied photovoltaic inverter systems in [25].

V. Conclusion

This paper developed a generalized method for converting dq impedance model of grid-tied VSC system into its SISO sequence domain equivalents. The converting process includes two steps: firstly converts dq impedance into its MIMO sequence domain equivalent, then converts the MIMO sequence domain equivalent into its SISO equivalent by means of closed-loop analysis method proposed in this paper. The decoupled SISO model allows the classic Nyquist Criterion to be used for stability analysis.

Two types of SISO model were given, the accurate one is directly from the consequence of conversion, and the reduced one is derived with a strong grid condition approximation. Numerical and time domain analysis shown that the reduced SISO model gives the wrong stability conclusions in cases where the system is highly dq asymmetric. On the contrary, the accurate SISO model presents a good consistence with MIMO model in terms of stability conclusions, particularly for the marginally stable condition.

The proposed method is general for any MIMO LTI systems. Therefore it is applicable to grid-tied VSC systems where a power controller or DC voltage controller is adopted. Only the marginal stability condition is proven to be identical in this work. Performance on gain and phase margin should be carefully evaluated in future works.

Appendix

A. Circuit Parameters Used in Stability Analysis and Simulations

TABLE A1
Circuit Parameters of the Grid-Tied VSC System

NAME	VALUES	NAME	VALUES
Nominal rating	2 MVA	Filter inductance	0.1 p.u.
Nominal voltage	0.69 kV	Grid inductance (SCR = 4)	1/SCR = 0.25 p.u.
Dc voltage	1.1 kV	Current controller (CC = 200 Hz)	$k_{\mathrm{p}}^{\mathrm{c}} = 0.03, k_{\mathrm{i}}^{\mathrm{c}} = 6.1$
Switching frequency	2.4 kHz	PLL controller (PLL = 20 Hz)	$k_{\mathrm{p}}^{\mathrm{pll}} = 71, k_{\mathrm{i}}^{\mathrm{pll}} = 1421$
		asymmetric grid controller	$k_{\mathrm{p}}^{\mathrm{v}} = 1, k_{\mathrm{i}}^{\mathrm{v}} = 100$

B. Modeling of Actively Controlled Grid

The dq domain grid model with control scheme in Fig. 6 is:

$$\mathbf{Z}_{\mathrm{grid}}^{\mathrm{dq}}(s)=\begin{bmatrix}1+\cos\delta_0 H_{\mathrm{v}}(s) & 0\\ -\sin\delta_0 H_{\mathrm{v}}(s) & 1\end{bmatrix}\begin{bmatrix}sL_{\mathrm{s}}+R_{\mathrm{s}} & -\omega_{\mathrm{s}}L_{\mathrm{s}}\\ \omega_{\mathrm{s}}L_{\mathrm{s}} & sL_{\mathrm{s}}+R_{\mathrm{s}}\end{bmatrix} \tag{A.1}$$

where δ_0 is the steady voltage angle difference between PCC and grid. Clearly, the dq impedance of actively controlled grid is not symmetric. Using the decomposition method in Section II-B gives a coupled sequence impedance:

$$\mathbf{Z}_{\mathrm{grid}}^{\mathrm{PN}}(s)=\mathbf{A}\mathbf{Z}_{\mathrm{grid}}^{\mathrm{dq}}(s)\mathbf{A}^{-1} \tag{A.2}$$

C. dq Symmetric and Asymmetric

For a dq impedance matrix $\left[\begin{smallmatrix}\mathrm{Z}^{\mathrm{dd}}(s) & \mathrm{Z}^{\mathrm{dq}}(s)\\ \mathrm{Z}^{\mathrm{qd}}(s) & \mathrm{Z}^{\mathrm{qq}}(s)\end{smallmatrix}\right]$, it is said to be dq symmetric if $\mathrm{Z}^{\mathrm{dd}}(s)=\mathrm{Z}^{\mathrm{qq}}(s)$ and $\mathrm{Z}_{\mathrm{dq}}(s)=-\mathrm{Z}_{\mathrm{qd}}(s)$, and if the condition not satisfied, the system is referred to dq asymmetric. For a dq symmetric system, its sequence equivalent can be obtained by linear transformation using the methods in Section II. As a result, the sequence impedance is decoupled. Otherwise, the sequence impedance is coupled.

References

[1] R. Teodorescu, M. Liserre, and P. Rodriguez, "Introduction," in *Grid Converters for Photovoltaic and Wind Power Systems*. Chichester, U.K.: Wiley, 2011, pp. 1–4.

[2] N. Flourentzou, V. G. Agelidis, and G. D. Demetriades, "VSC-Based HVDC power transmission systems: An overview," *IEEE Trans. Power Electron*, vol. 24, no. 3, pp. 592–602, Mar. 2009.

[3] D. Dong, B. Wen, D. Boroyevich, P. Mattavelli, and Y. Xue, "Analysis of phase-locked loop low-frequency stability in three-phase grid-connected power converters considering impedance interactions," *IEEE Trans. Ind. Electron.*, vol. 62, no. 1, pp. 310–321, Jan. 2015.

[4] L. P. Kunjumuhammed, B. C. Pal, C. Oates, and K. J. Dyke, "Electrical oscillations in wind farm systems: Analysis and insight based on detailed modeling," *IEEE Trans. Sustain. Enery*, vol. 7, no. 1, pp. 51–62, Jan. 2015.

[5] D. Yang, X. Ruan, and H. Wu, "Impedance shaping of the grid-connected inverter with LCL filter to improve its adaptability to the weak grid condition," *IEEE Trans. Power Electron*, vol. 29, no. 11, pp. 5795–5805, Nov. 2014.

[6] L. Harnefors, M. Bongiorno, and S. Lundberg, "Input-admittance calculation and shaping for controlled voltage-source converters," *IEEE Trans. Ind. Electron.*, vol. 54, no. 6, pp. 3323–3334, Dec. 2007.

[7] M. Belkhayat, "Stability criteria for AC power systems with regulated loads," Ph.D. dissertation, Dept. Elec. Eng., Purdue University, West Lafayette, IN, USA, 1997.

[8] M. Cespedes and J. Sun, "Impedance modeling and analysis of grid-connected voltage-source converters," *IEEE Trans. Power Electron.*, vol. 29, no. 3, pp. 1254–1261, Mar. 2014.

[9] B. Wen, D. Boroyevich, R. Burgos, P. Mattavelli, and Z. Shen, "Small-signal stability analysis of three-phase AC systems in the presence of constant power loads based on measured d-q, frame impedances," *IEEE Trans. Power Electron.*, vol. 30, no. 10, pp. 5952–5963, Oct. 2015.

[10] S. Shah and L. Parsa, "On impedance modeling of single-phase voltage source converters," in *Proc. IEEE Energy Convers. Congr. Expo.*, 2016, pp. 1–8.

[11] J. Lyu, X. Cai, and M. Molinas, "Impedance modeling of modular multilevel converters," in *Proc. Annu. Conf. IEEE Ind. Electron. Soc.*, Yokohama, Japan, 2015, pp. 180–185.

[12] J. Sun, "Small-signal methods for AC distributed power systems–A review," in *Proc. IEEE Electr. Ship Technol. Symp.*, 2009, pp. 44–52.

[13] E. Möllerstedt, "Dynamic analysis of harmonics in electrical systems," Ph.D. dissertation, Dept. Automat. Control, Lund University, Lund, Sweden, 2000.

[14] M. K. Bakhshizadeh *et al.*, "Couplings in phase domain impedance modeling of grid-connected converters," *IEEE Trans. Power Electron*, vol. 31, no. 10, pp. 6792–6796, Oct. 2016.

[15] S. Shah and L. Parsa, "Sequence domain transfer matrix model of three-phase voltage source converters," in *Proc. IEEE Power Energy Soc. General Meet.*, 2016, pp. 1–5.

[16] L. Harnefors, "Modeling of three-phase dynamic systems using complex transfer functions and transfer matrices," *IEEE Trans. Ind. Electron*, vol. 54, no. 4, pp. 2239–2248, Aug. 2007.

[17] A. Rygg, M. Molinas, C. Zhang, and X. Cai, "A modified sequence domain impedance definition and its equivalence to the dq-domain impedance definition for the stability analysis of ac power electronic systems," *IEEE J. Emerg. Sel. Topics Power Electron.*, vol. 4, no. 4, pp. 1382–1396, Dec. 2016.

[18] G. C. Paap, "Symmetrical components in the time domain and their application to power network calculations," *IEEE Trans. Power Syst*, vol. 15, no. 2, pp. 522–528, May 2000.

[19] X. Wang, L. Harnefors, F. Blaabjerg, and P.C. Loh, "A unified impedance model of voltage-source converters with phase-locked loop effect," in *Proc. IEEE Energy Convers. Congr. Expo.*, 2016, pp. 1–8.

[20] J. Kwon, X. Wang, F. Blaabjerg, C. L. Bak, V. S. Sularea, and C. Busca, "Harmonic interaction analysis in grid-connected converter using Harmonic State Space (HSS) modeling," *IEEE Trans. Power Electron.*, vol. 32, no. 9, pp. 6823–6835, Sep. 2016.

[21] C. Desoer and Y.T. Wang, "On the generalized nyquist stability criterion," *IEEE Trans. Autom. Control*, vol. 25, no. 2, pp. 187–196, Apr. 1980.

[22] C. Zhang, X. Cai, Z. Li, A. Rygg, and M. Molinas, "Properties and physical interpretation of the dynamic interactions between voltage source converters and grid: Electrical oscillation and its stability control," *IET Power Electron.*, vol. 10, no. 8, pp. 894–902, Jun. 2017.

[23] J. Sun, "Impedance-based stability criterion for grid-connected inverters," *IEEE Trans. Power Electron*, vol. 26, no. 11, pp. 3075–3078, Nov. 2011.

[24] L. Harnefors, X. Wang, A. G. Yepes, and F. Blaabjerg, "Passivity-based stability assessment of grid-connected VSCs—An overview," *IEEE J. Emerg. Sel. Topics Power Electron.*, vol. 4, no. 1, pp. 116–125 Mar. 2016.

[25] C. Li, "Unstable operation of photovoltaic inverter from field experiences," *IEEE Trans. Power Del*, to be published, doi: 10.1109/TPWRD.2017.2656020.

Chen Zhang received the B.Eng. degree in electrical engineering from China University of Mining and Technology, Xuzhou, China, in 2011. He is currently working toward the Ph.D. degree in electrical engineering with Shanghai Jiao Tong University, Shanghai, China. He was a Ph.D. Visiting Scholar in the Department of Engineering Cybernetics, Norwegian University of Science and Technology, Trondheim, Norway, in 2015. His current research interests include modeling and stability analysis of VSC-based energy conversion systems, where the aim is to reveal the fundamental dynamics and stability mechanisms of renewable energies with VSCs as the grid interface.

Xu Cai received the B.Eng. degree from Southeast University, Nanjing, China, in 1983, and the M.Sc. and Ph.D. degrees from China University of Mining and Technology, Xuzhou, China, in 1988 and 2000, respectively. He was in the Department of Electrical Engineering, China University of Mining and Technology, as an Associate Professor, from 1989 to 2001. He was the Vice Director of the State Energy Smart Grid R&D Center, Shanghai, China, from 2010 to 2013. He has been with Shanghai Jiao Tong University, Shanghai, as a Professor, since 2002, where he has also been the Director of the Wind Power Research Center, since 2008. His current research interests include power electronics and renewable energy exploitation and utilization, including wind power converters, wind turbine control system, large power battery storage systems, clustering of wind farms and its control system, and grid integration.

Atle Rygg received the M.Sc. degree in electrical engineering from Norwegian University of Science and Technology (NTNU), Trondheim, Norway, in 2011. He is currently working toward the Ph.D. degree in Department of Engineering Cybernetics at NTNU. From 2011 to 2015, he was a Research Scientist at SINTEF Energy Research in the field of power electronics. His topic or research interests include impedance based stability analysis of power electronic systems, where the aim is to contribute to the fundamental understanding in this family of methods.

Marta Molinas (M'94) received the Diploma degree in electromechanical engineering from the National University of Asuncion, Asuncion, Paraguay, in 1992, the Master of Engineering degree from Ryukyu University, Nishihara, Japan, in 1997, and the Doctor of Engineering degree from Tokyo Institute of Technology, Tokyo, Japan, in 2000. She was a Guest Researcher with the University of Padova, Padova, Italy, during 1998. From 2004 to 2007, she was a Postdoctoral Researcher with the Norwegian University of Science and Technology (NTNU) and from 2008 to 2014 she has been Professor in the Department of Electric Power Engineering at the same university. She is currently a Professor in the Department of Engineering Cybernetics, NTNU. Her research interests include stability of power electronics systems, harmonics, instantaneous frequency, and nonstationary signals from the human and the machine. She is an Associate Editor for the IEEE JOURNAL OF EMERGING AND SELECTED TOPIC IN POWER ELECTRONICS, the IEEE TRANSACTIONS ON POWER ELECTRONICS and an Editor of the IEEE TRANSACTIONS ON ENERGY CONVERSION. She has been an AdCom Member of the IEEE Power Electronics Society from 2009 to 2011.